Effect of Ti on Phase Transformation and Grain Evolution in Nb/V Microalloyed Steel


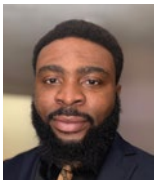


Low-carbon Nb/V microalloyed steels are used extensively for pipeline construction due to a good combination of mechanical properties and weldability. Austenite/ferrite transformation and grain size evolution during cooling after hot rolling is pivotal to obtaining desired properties. In this study, phase transformation and grain size evolution in two as-cast Nb/V microalloyed low-carbon steel billets were investigated with and without Ti additions, utilizing a quenching dilatometer. Significant ferrite grain morphology changes were observed in Ti-added steel at 10 and 1°C/second cooling rates. Mechanisms of observed changes were discussed and compared with thermodynamic/kinetic predictions.

Authors

Barshan Saha (top right), Graduate Research Assistant Peaslee Steel Manufacturing Research Center, Department of Materials Science and Engineering, Missouri University of Science and Technology, Rolla, Mo., USA
barshan.saha@mst.edu

Henry Haffner (top middle), Department of Mechanical and Aerospace Engineering, Missouri University of Science and Technology, Rolla, Mo., USA

Mario Buchely (top left), Roberta and G. Robert Couch Assistant Professor, Peaslee Steel Manufacturing Research Center, Department of Materials Science and Engineering, Missouri University of Science and Technology, Rolla, Mo., USA
buchelym@mst.edu

Simon Lekakh (bottom left), Professor, Peaslee Steel Manufacturing Research Center, Department of Materials Science and Engineering, Missouri University of Science and Technology, Rolla, Mo., USA

K. Chandrashekhara, Department of Mechanical and Aerospace Engineering, Missouri University of Science and Technology, Rolla, Mo., USA

Ronald J. O'Malley (bottom right), F. Kenneth Iverson Chair of Steelmaking Technologies, Director Peaslee Steel Manufacturing Research Center, Department of Materials Science and Engineering, Missouri University of Science and Technology, Rolla, Mo., USA
omalleyr@mst.edu

Introduction

Microalloyed steels represent a unique class of advanced materials that offer a combination of high strength and good formability and are also designed to have greater resistance to atmospheric corrosion than low-carbon steels.[1] This steel grade is also called high-strength low-alloy (HSLA) steel. The chemistry of HSLA steels typically involves controlled amounts of alloying elements such as Mn, Mo, Si, Nb, V, Ti, etc. However, Nb, V and Ti are the most common microalloying elements for HSLA steels because of the grain refinement of their carbonitrides that make the precipitation behavior complex.[2,3] Nb,V carbides/carbonitrides in austenite inhibit the static recrystallization of austenite, thus resulting in finer microstructure. Moreover, Ti is frequently introduced to HSLA steels for enhancing the control of the austenite and transformed ferrite grain size during deformation and heat treatments.[4,5]

Acicular ferrite has been an optimal microstructure for its combination of strength and toughness, which is a more suitable candidate for pipeline steel in a severe environment. The interlocking microstructure of acicular ferrite resists the crack propagation which provides increased strength and toughness. The acicular ferrite microstructure in low-carbon Mn-Nb is formed during the continuous cooling process, where both shear transformation and diffusion mechanics coexist in a specific temperature range slightly higher than the upper bainite. Due to the needlelike ferrite morphology, it is also referred to as bainite.[6,7]

Among all the microalloying elements, Ti-containing inclusions provide suitable intragranular nucleation sites for acicular ferrite.

Table 1

Chemical Composition of as-cast Nb, V Microalloyed Steel Samples

Material		C	Mn	Si	Al	Nb	V	Ti	N
A	min	0.040	1.400	0.180	0.018	0.045	0.035	0.005	—
	max	0.052	1.600	0.300	0.050	0.060	0.060	0.020	0.100
B	min	0.039	1.100	0.190	0.019	0.030	0.030	—	—
	max	0.070	1.350	0.300	0.050	0.050	0.050	—	0.100

Grain refinement usually depends on multiple factors such as chemistry, density, inclusion size and lattice mismatch. From previous studies, it has been reported that the activation energy for nucleation of intragranular ferrite is inversely proportional to inclusion diameter. Moreover, nonmetallic inclusions less than 100 nm in size are capable of grain refinement by forming fine Mn-Ti complex oxides for ferrite nucleation and thus pinning the grain boundaries.[8–14]

The study of bainite/acicular ferrite transformation and the concept of continuous cooling transformation (CCT) diagrams are of utter importance for proper design of a microalloyed pipeline steel. From the CCT diagrams, ferrite transformation can be studied. However, it cannot distinguish between polygonal ferrite, quasi-polygonal ferrite and acicular ferrite, which are critically important for a better understanding of the microalloyed steel. Therefore, an experimental phase transformation is required by which all the phase transformations (different ferrite, bainite, pearlite) occur during cooling from the austenite region. Dilatometry, differential thermal analysis (DTA) or differential scanning calorimetry (DSC) can be used for the required thermomechanical testing. In addition, bainite/acicular ferrite phase transformation can also be confirmed by optical microscope (OM) and scanning electron microscope (SEM).[15–21] In this article, an experimental approach is implemented to study the effect of Ti on acicular ferrite/bainite phase transformation in Nb, V microalloyed steel for the pipeline application.

Experimental Procedure

Two industrially processed microalloyed steel slabs were used in this study. The chemical composition of each grade is presented in Table 1. The material was obtained from a thin caster, in the as-cast condition. Both grades are Nb,V microalloyed steel; Material A was also microalloyed with Ti, whereas Material B was not Ti microalloyed. The as-received slabs were 8 inches long, 8 inches wide and 2.5 inches thick. After the sectioning and grinding, cylindrical samples of ϕ3 mm (~0.12 inch) × 10 mm (~0.39 inch) were extracted from the 1/4 thickness section of the slab using Maxiem 0707 water-jet cutter.

The cylindrical samples were characterized by dilatometry to obtain the phase transformation in these materials. The Linseis DIL L78 Rita quenching dilatometer was used for this purpose. During a dilatometry test, the cylinders were held at 1,200°C for 2 minutes to austenitize the sample, followed by holding at 1,000°C for 1 minute to homogenize the system before controlled cooling to room temperature at 100°C/second, 10°C/second, 1°C/second and 0.1°C/second. A schematic of the heat and cooling cycle is shown in Fig. 1. Notice that double austenitization cycle was performed during this experiment. This was done due to calibration of the equipment showing better dilatometry results after the first heating/cooling cycle. For minimizing oxidation on the surface of the sample, the whole experiment was performed under a high-purity helium gas atmosphere for faster cooling rate and high-purity argon gas atmosphere for slower cooling rate.

Figure 1

Schematic of the heating and cooling cycle used in the dilatometer.

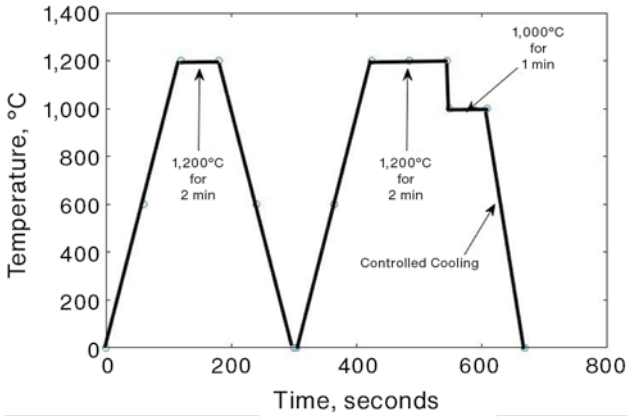

Figure 2

JMatPro predictions in Material A (with-Ti): major phases (a) and minor phases (b).

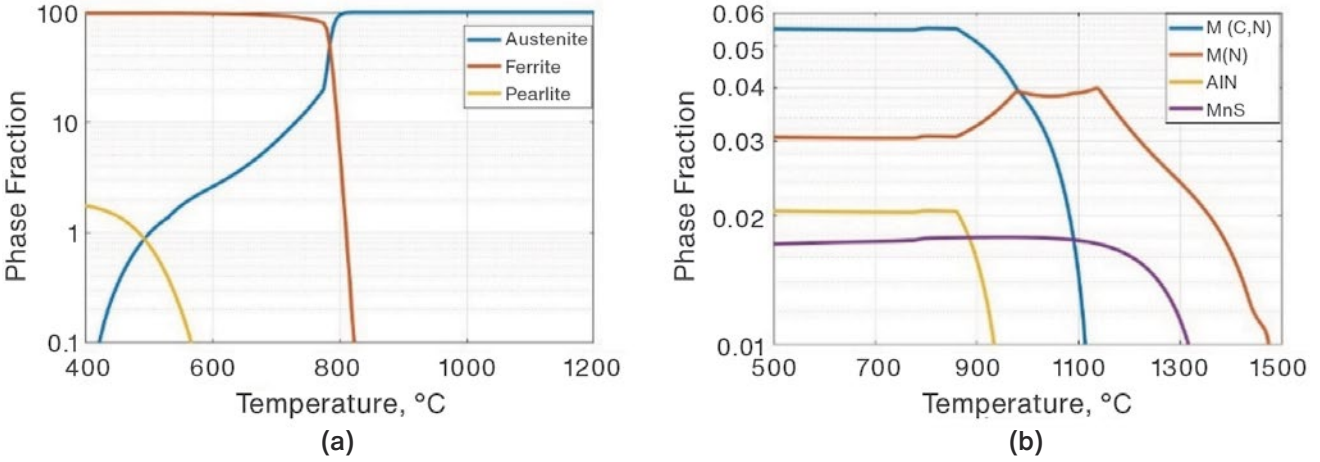

After dilatometry, cylinders were carefully sectioned into the middle portion and prepared for metallographic analysis. After polishing, the material was etched with 2% Nital. Polished samples were characterized by Nikon Epiphot light optical microscope (LOM).

MATLAB software was used for analyzing and processing dilatometric data. Thus, the phase transformation curve was plotted, and critical temperatures characterized using first derivative criteria. Additionally, JMatPro simulation was performed to predict the present phases along with CCT curve.

Results and Discussion

Phase Stability by JMatPro Simulations

Fig. 2 shows phase predictions upon cooling for Material A (with Ti). According to these predictions, the phases at room temperature will be mostly ferrite and a small amount of pearlite under equilibrium conditions. From the austenite phase, the ferrite phase appears at 830°C. Later, at 565°C, pearlite is visible before austenite is fully transformed. It is also noted that upon heating, AlN, Nb, V, Ti and carbonitrile fully dissolve at 875°C and 900°C, respectively, which could act as a pinning agent of the austenitic grains. However, it takes more than 1,100°C to dissolve complex metal nitrides and MnS in the solution. Therefore, 1,200°C was chosen for the full austenitization of this sample in the dilatometer.

Likewise, Fig. 3 shows phase predictions upon cooling for Material B (without Ti). Like Material A, both ferrite and pearlite phase are present in the room temperature. From the austenite phase, the ferrite phase appears at 830°C. Later, at 590°C, pearlite appears. Nb,V carbide-nitrides dissolve at 900°C. Other minor phases such as AlN and MnS are dissolved at 1,000°C and 1,100°C, respectively, according to these simulations.

Figure 3

JMatPro predictions in Material B (without Ti): major phases (a) and minor phases (b).

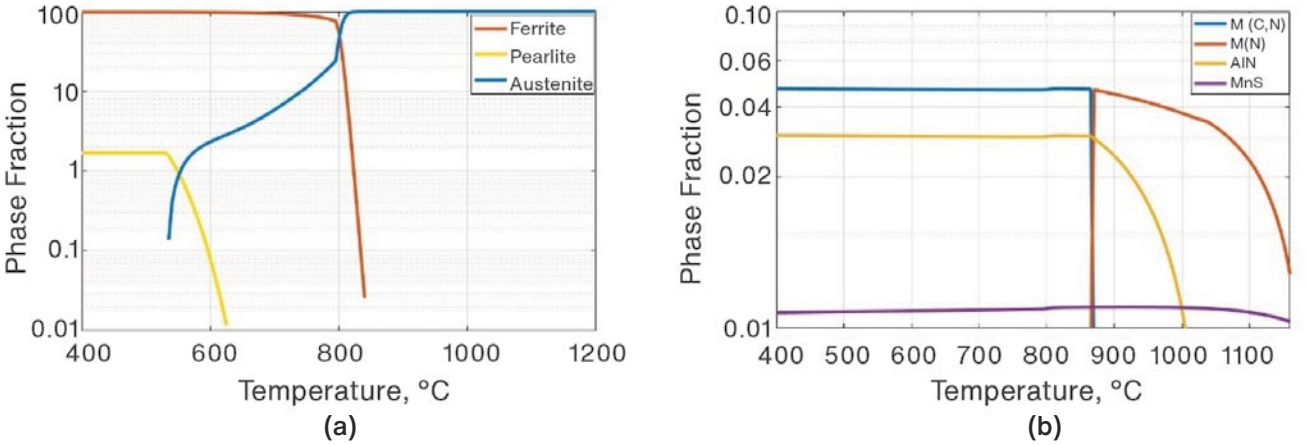

Figure 4

As-received microstructures of Material A (a) and Material B (b), in as-cast condition. PF: Polygonal ferrite, QF: Quasi-Ferrite, AF: Acicular Ferrite using optical microscope.

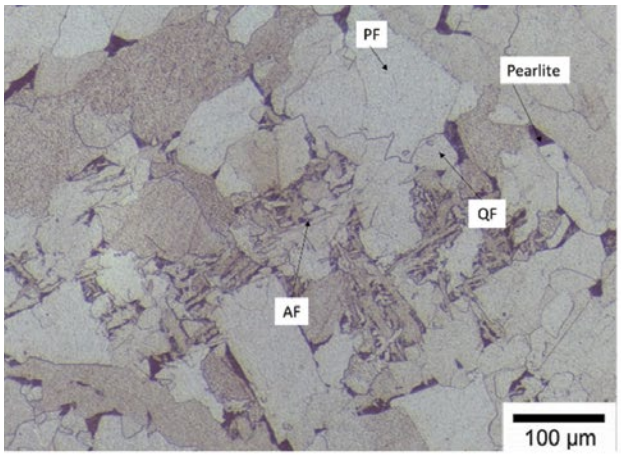

(a)

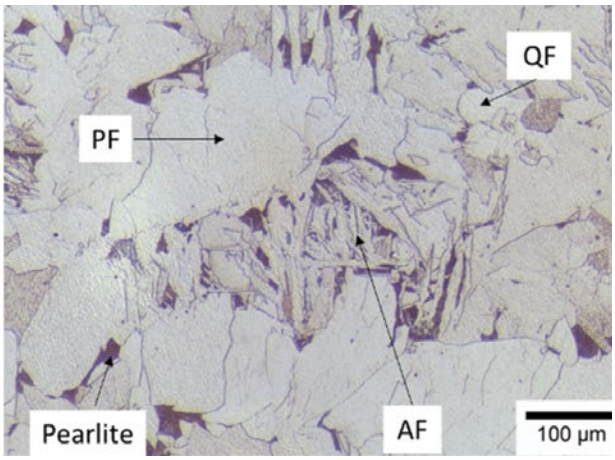

(b)

Figure 5

Continuous cooling transformation from JMatPro simulation.

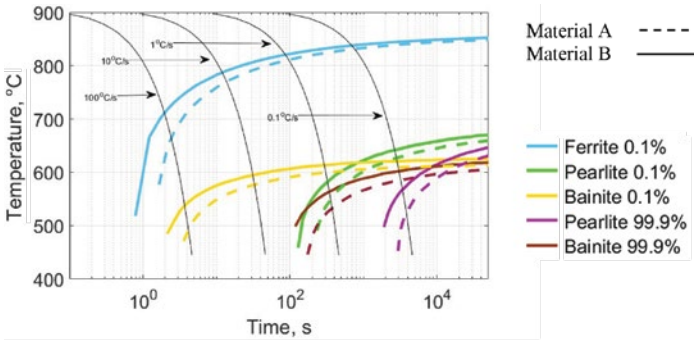

As-Received Material: As-Cast Condition

Fig. 4 shows optical microscopic images of the as-received Nb,V microalloyed steel, both Material A (with Ti) and Material B (without Ti). From these micros, it is evident that both allotriomorphic ferrite and pearlite are present in the as-cast microstructures. In this condition, bainite looks more like acicular ferrite morphology. The exact cooling path was not provided for this material; thus, the observed acicular morphologies are difficult to explain. Another observation is that, tracking the ferrite grains, it was possible to see that the prior austenitic grains were of the order to ~100 µm.

Figure 6

Dilatometric analysis: Example of dilatometric curves for Material A (a), and example of analysis of data in dilatometric curve to calculate fraction of transformed phase (b).

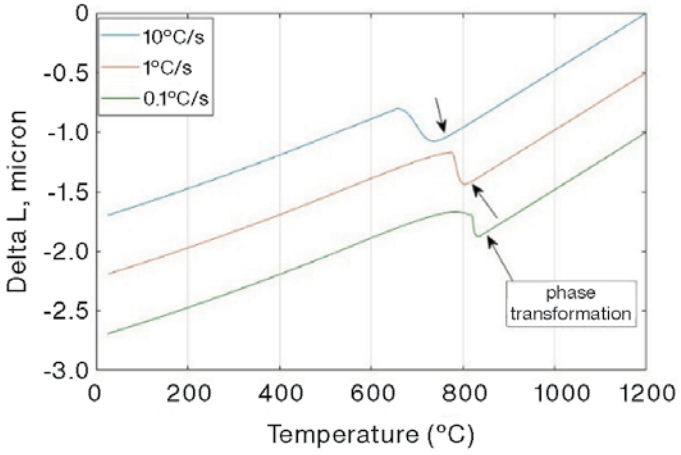

(a)

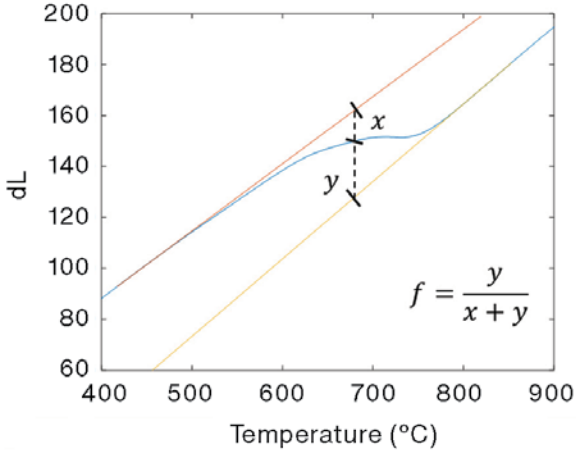

(b)

Figure 7

Experimental phase transformation of Material A (with Ti) and Material B (without Ti).

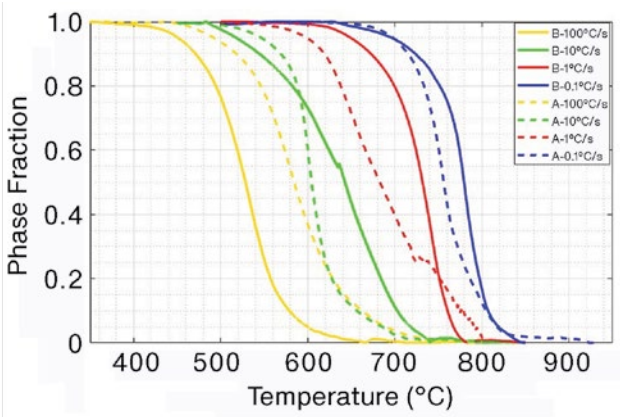

Continuous Cooling Transformation Simulation

Fig. 5 shows CCT curves for both materials obtained by JMatPro, and assuming a prior austenitic grain size (PAGS) of 100 µm. Austenitizing temperature is predicted to be 907°C. The martensite start temperature (Ms) of Material A (with Ti) is found to be 445°C, whereas Ms of Material B is 456°C. It is also observed that bainite is present even in the faster cooling rate such as 100°C/second, along with intermediate cooling rate of 10°C/second and 1°C/second, whereas pearlite is formed along with bainite in slow cooling such as 0.1°C/second. Also, allotriomorphic ferrite is observed at 0.1°C/second. However, the presence of Ti delays the bainite and pearlite transformation during continuous cooling.

Dilatometric Results

Fig. 6 shows examples of dilatometric curve upon cooling obtained from the studied materials. From these curves,

Figure 8

Microstructures of Material A (left) and Material B (right) in 100°C/second condition using optical microscope.

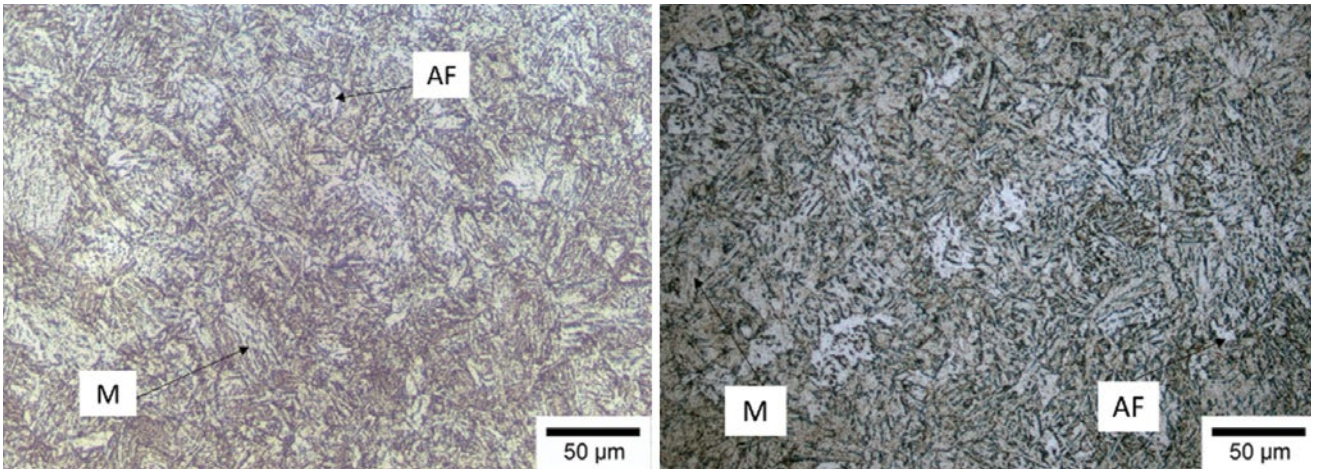

Figure 9

Microstructures of Material A (left) and Material B (right) in 10°C/second condition using optical microscope.

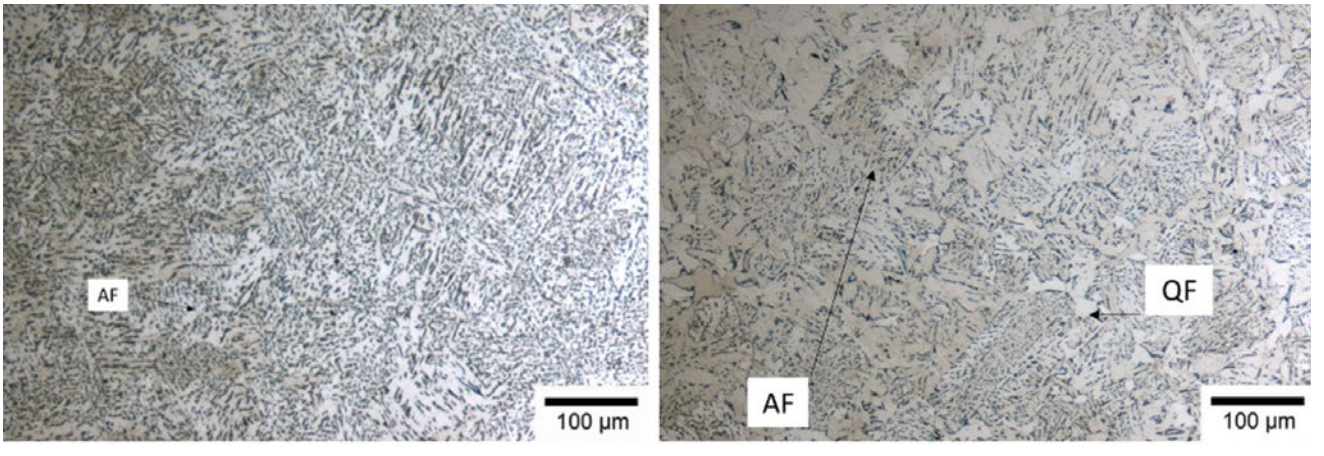

the phase fraction of transformation was extracted using lever rule criteria, as schematically shown in Fig. 6b. For this purpose, a MATLAB code was developed; then, the phase fraction curves from Fig. 7 were obtained.

From Fig. 8 to Fig. 11, microstructures of both materials after continuous cooling (100, 10, 1 and 0.10°C/second, respectively) are shown. Experimentally at 100°C/second condition, Fig. 8 shows both martensite (M) – acicular ferrite (AF) morphologies were obtained from both materials. From the JMatPro calculation (Fig. 5), it was predicted that there would be M, but also ferrite and bainite at 100°C/second. Bainite is not clearly observed in this magnification, but certainly the other two phases (M and AF) are present in the microstructure. From the micrograph at 10°C/second condition (Fig. 9), it was observed that mostly AF was obtained in Material A (with Ti), whereas a small portion of quasi-polygonal ferrite (QF) is evident along the grain boundaries in Material B (without Ti). Additionally, it seems that the Ti microalloyed material A promoted finer and more consistent AF morphology than the material B. Compared to the JMatPro calculation (Fig. 5), ferrite and bainite phase were also predicted for this cooling rate, where bainitic transformation occurred at ~583°C. This temperature is not fully evident from the experimental phase transformation curves (Fig. 7); and bainite cannot been observed in the microstructures, at least in the magnification obtained in the LOM.

From Fig. 10, the difference of morphology is clearly visible in the case of 1°C/second. There is more than one ferrite morphology in both microstructures. Material A has a higher percentage of AF, and some QP and

Figure 10

Microstructures of Material A (left) and Material B (right) in 1°C/second condition using optical microscope.

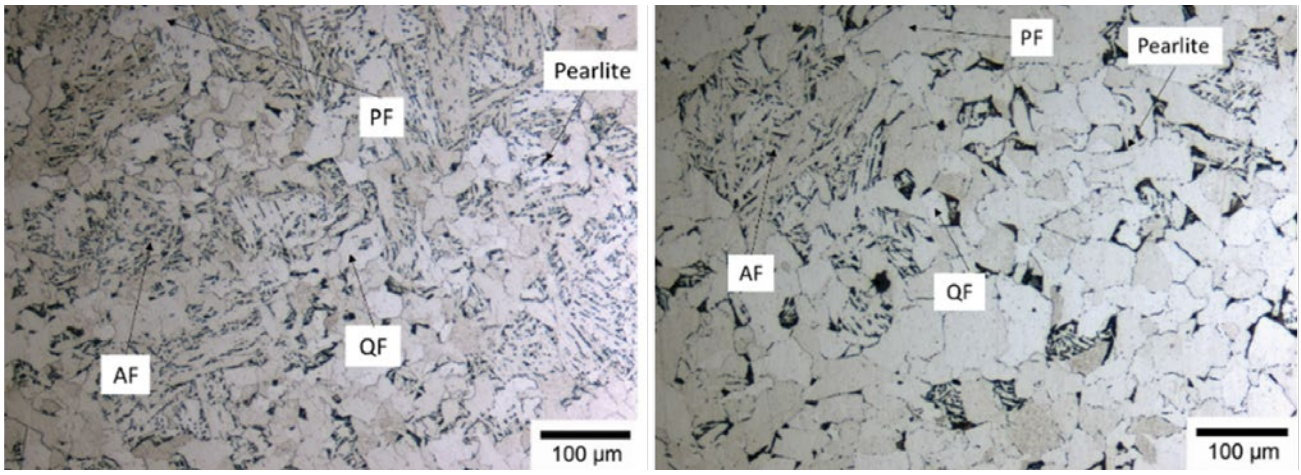

Figure 11

Microstructures of Material A (left) and Material B (right) in 0.1°C/second condition using optical microscope.

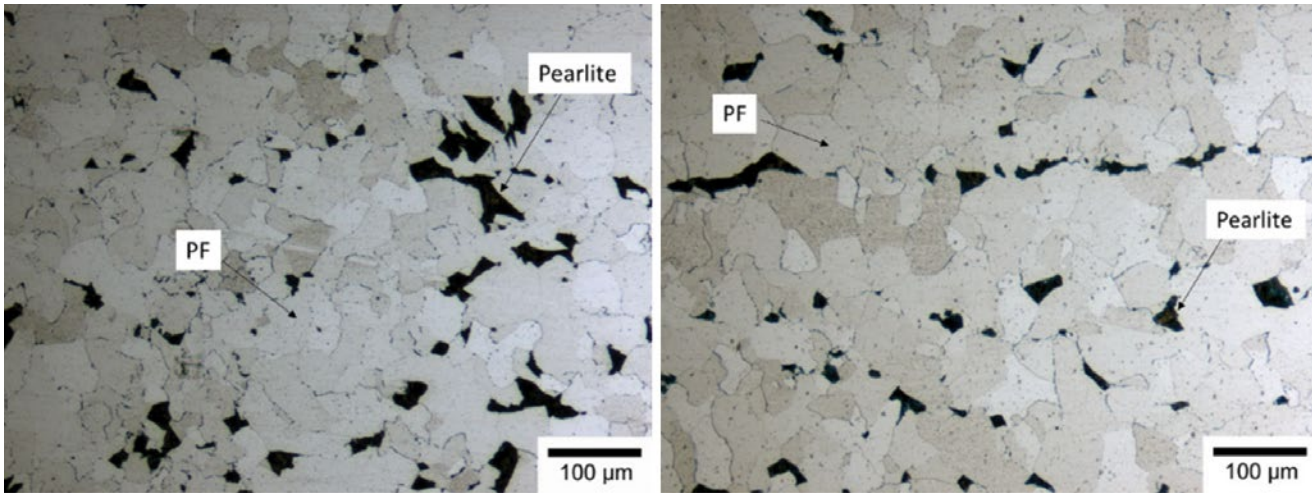

polygonal ferrite (PF) and pearlite were also observed. In the case of Material B, there is a higher fraction of PF over AF. Also, the proportion of pearlite is higher in Material B. Moreover, tracking the PF, it can be seen that there were dissimilarities in the PAGS for both materials. The sample without Ti showed larger PAGS than the samples with Ti. This effect could be explained due to the TiN, and (Nb, V, Ti)(C, N) are more stable at higher temperatures and could serve as pinning agents and inhibit the grain growth.

Uniform ferrite-pearlite microstructures were observed at the slowest (0.1°C/second) cooling rate condition, as shown in Fig. 11. Both phases were predicted by JMatPro calculations (Fig. 5) at this cooling rate. Also, it seems that the ferrite grains are smaller in Material A compared to Material B. This effect could also be explained by the smaller PAGS obtained in Material A due to the presence of TiN as a pinning agent.

Using the experimental curves presented in Fig. 7, different transitions were established, and comparing microstructures, the experimental CCT curve shown in Fig. 12 was built for both materials. Bainite transformation temperature was not determined due to the lack of evidence in the microstructures, perhaps due to the low resolution of the LOM to clearly observe bainite.

Notice that different ferrite morphologies were extrapolated from the experimental results, including PF, quasi-polygonal ferrite (QF) and acicular ferrite (AF). Compared to the JMatPro calculations (Fig. 5), ferrite was predicted in a similar range of temperatures shown in Fig. 12, but the calculation did not distinguish among different ferrite morphologies. Thus, the value of this work is to understand that for these types of steel grades, different morphologies can be obtained, and they must be experimentally determined. The final observation from Fig. 12 is that the acicular and quasi-ferrite formation is delayed with the Ti addition of Material A. This effect was partially observed in the JMatPro predictions. However, at a low cooling rate of 0.1°C/second, the PF seems to revert the effect and precipitate earlier in Material A. This effect can be explained due to the smaller PAGs observed in Material A. Smaller austenitic grains could promote more nucleation sites for stable PF, and that could be the reason why, at lower cooling rates, the PF appears at higher temperatures in Material A than in B.

Figure 12

Experimental CCT with modified phase region.

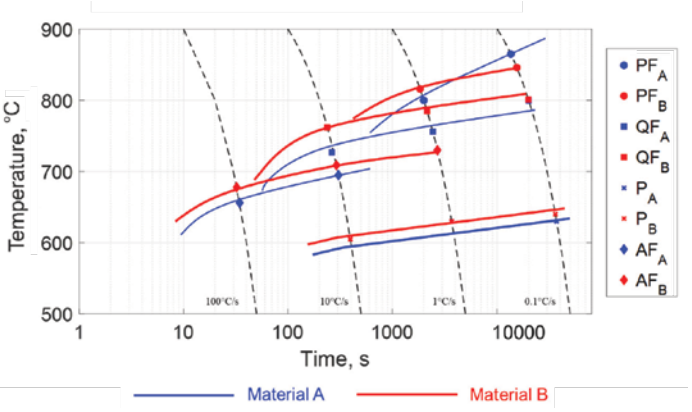

Conclusion

The current work examined the effect of Ti on acicular, quasi, polygonal ferrite and pearlite phase transformation through simulated and experimental heat treatments with four different controlled cooling condition using quenching dilatometer. Two Nb,V microalloyed steel grades, one with Ti additions (Material A), and other without Ti additions (Material B), were used to perform dilatometric and microstructural studies. Based on the experimental and simulated data analysis, the following conclusions were found:

- Higher cooling rate (>100°C/second) promoted martensitic transformation, and the microstructures are a mixture of martensitic and acicular ferrite.
- Higher cooling rate (~10°C/second) also favored the formation of nonpolygonal ferrite such as acicular and quasi ferrite.
- Intermediate cooling rate resulted in a range of ferrite morphology such as acicular, quasi and polygonal along with pearlite.
- Adding Ti was responsible for finer acicular ferrite.
- Addition of Ti was also responsible for delaying the acicular and quasi-ferrite transformation, specifically at cooling rates higher than 1°C/second.
- Formation of TiN and complex Nb, V, Ti (C, N) precipitation acted as pinning agent, which resulted in grain refinement.
- Predictions by JMatPro could explain some transition temperatures, but it does not account for different ferrite morphologies that can be obtained in this type of microalloyed steels.

Acknowledgment

This research was funded by the sponsors of the Peaslee Steel Manufacturing Research Center, and industry/university cooperative research center. The authors are grateful to Richard Osei, Dimitry Tsvetkov and Ping Wei from Steel Dynamics Inc. for providing the experimental materials.

References

1. H.K.D.H. Bhadeshia and R. Honeycomb, *Steels Microstructure and Properties,* 3rd ed., Elsevier, 2006.
2. S.W. Thompson, D.J. Colvin and G. Krauss, *Metal. Mater. Trans.,* Vol. 27A, 1996, pp. 1557–1571.
3. S.W. Thompson and G. Krauss, *Metal. Mater. Trans.,* Vol. 27A, 1996, pp. 1573–1588.
4. P. Gong, E.J. Palmiere and W.M. Rainforth, "Dissolution and Precipitation Behaviour in Steels Microalloyed With Niobium During Thermomechanical Processing," *Acta Mater,* Vol. 97, 2015, pp. 392–403.
5. J. Webel, A. Herges, D. Britz et al., "Tracing Microalloy Precipitation in Nb-Ti HSLA Steel During Austenite Conditioning," *Metals,* Vol. 10, No. 2, 2020, pp. 1–22.
6. Furen Xiao, Bo Liao, Deliang Ren et al., "Acicular Ferritic Microstructure of a Low-Carbon Mn–Mo–Nb Microalloyed Pipeline Steel," *Materials Characterization,* Vol. 54, No. 4-5, 2005, pp. 305–314.
7. S.S. Babu and H.K.D.H. Bhadeshia, "Stress and The Acicular Ferrite Transformation," *Material Science and Engineering A,* Vol. 156, 1992, pp. 1–9.
8. M. Fattahi, N. Nabhani et al., "Effect of Ti-Containing Inclusions on the Nucleation of Acicular Ferrite and Mechanical Properties of Multipass Weld Metals," *Micron,* Vol. 45, 2013, pp. 107–114.
9. S.S. Babu, "The Mechanism of Acicular Ferrite in Weld Deposits," *Current Opinion in Solid State and Materials Science,* Vol. 8, No. 3–4, 2004, pp. 267–278.
10. J-S. Byun, J-H. Shim et al., "Non-Metallic Inclusion and Intragranular Nucleation of Ferrite in Ti-Killed C–Mn Steel," *Acta Materialia,* Vol. 51, No. 6, 2003, pp. 1593–1606.
11. M. Gomez, P. Valles et al., "Evolution of Microstructure and Precipitation State During Thermomechanical Processing of a X80 Microalloyed Steel," *Materials Science and Engineering A,* Vol. 528, 2011, pp. 4761–4773.
12. J.H. Shim, Y.J. Oh et al., "Ferrite Nucleation Potency of Non-Metallic Inclusions in Medium Carbon Steels," *Acta Materialia,* Vol. 49, 2001, pp. 2115–2122.
13. Y. Yang, X. Jia et al., "Effect of Nb on Microstructure and Mechanical Properties Between Base Metal and High Heat Input Coarse-Grain HAZ in a Ti-Deoxidized Low Carbon High Strength Steel," *Journal of Materials Research and Technology,* Vol.18, 2022, pp. 2399–2412.
14. L. García-Sesma et al., "Effect of Coiling Conditions on The Strengthening Mechanisms of Nb Microalloyed Steels With High Ti Addition Levels," *Materials Science & Engineering A,* Vol. 748, 2019, pp. 386–395.
15. A. Grajcar, W. Zalecki et al., "Dilatometric Study of Phase Transformations in Advanced High-Strength Bainitic Steel," *Journal of Thermal Analysis and Calorimetry,* Vol. 118, 2014, pp. 739–748.
16. J.R. Yang and H.K.D.H. Bhadeshia, "Continuous Heating Transformation of Bainite to Austenite," *Materials Science and Engineering A,* Vol. 131, 1991, pp. 99–113.
17. M. Goji, M. Suceska, et al., "Thermal Analysis of Low Alloy Cr–Mo Steel," *Journal of Thermal Analysis and Calorimetry,* Vol. 75, 2004, pp. 947–956.
18. P.V. Morra, A.J. Böttger et al., "Decomposition of Iron-Based Martensite a Kinetic Analysis by Means of Differential Scanning Calorimetry and Dilatometry," *Journal of Thermal Analysis and Calorimetry,* Vol. 64, 2001, pp. 905–914.
19. R.Y. Zhang and J.D. Boyd, "Bainite Transformation in Deformed Austenite," *Metallurgical and Materials Transaction A,* Vol. 41, 2010, pp. 1448–1459.
20. H. Zhao and E.J. Palmiere, "Effect of Austenite Deformation on The Microstructure Evolution and Grain Refinement Under Accelerated Cooling Conditions," *Metallurgical and Materials Transactions A,* Vol. 48, 2017, pp. 3389–3399.
21. B. Bramfitt and J.G. Speer, "A Perspective on the Morphology of Bainite," *Metallurgical Transaction A,* Vol. 21, 1990, pp. 817–829.

AISTech This paper was presented at AISTech 2024 — The Iron & Steel Technology Conference and Exposition, Columbus, Ohio, USA, and published in the AISTech 2024 Conference Proceedings.

Did You Know?

SSAB Highlights Decarbonization Efforts at COP29

SSAB joined Business Sweden's delegation to the United Nations Climate Change Conference, COP29, in Baku, Azerbaijan in November, the company reported.

"SSAB believes that ambition and speed in the climate transition must increase. We need to phase out fossil fuels and it must cost to emit. Global carbon pricing mechanisms and common emission standards are needed to set the foundation for faster industrial decarbonization," Martin Pei, SSAB chief technology officer, said during the conference.

SSAB said it will highlight its efforts to decarbonize steel production by switching from coking coal to fossil-free electricity as the primary energy source. SSAB plans to transform its entire Nordic production system to carbon emission-free steelmaking using both recycled steel and virgin iron ore as the raw material.

"Creating internationally accepted trade rules for near zero-emission steel products would allow for significant global CO_2 emissions reductions by incentivizing the roll-out of clean steel production technologies," Pei said.